Research on the evolution trend of land subsidence induced by groundwater over-exploitation in Liaocheng city

Hao Liang[1], Yongwei Zhang[1], Xueyang Hu[2], Dejie Yu[1] and Chao Jia[2,*]

[1]Shandong Provincial Territorial Spatial Ecological Restoration Center, Jinan, Shandong, 250061, China.
[2]Institute of Marine Science and Technology, Shandong University, Qingdao, 266237, China

jiachao@sdu.edu.cn

Abstract. Based on hydrogeological data and years of land subsidence monitoring data in Liaocheng City, a 3D fluid-solid coupling numerical model of land subsidence in Liaocheng City were established. The model restored the evolution law of land subsidence caused by water extraction in the area, predicted the development trend of subsidence. Results show that (1) land subsidence in Liaocheng mainly occurs in four areas of Linqing, Guanxian, Chiping and Dong'a, and the subsidence rate is 30-50mm/a; (2) under the scenario of maintaining the current amount of groundwater extraction, land subsidence in Liaocheng will still develop in the next ten years and will reach 321 mm by 2031; (3) under the scenario of establishing no-mining zones, the subsidence will be reduced to 256 mm by 2031. It is proposed to set up no-mining zones in the eastern and northwestern part of Liaocheng to reasonably develop and utilize groundwater resources.

Keywords: land subsidence; simulation prediction; Liaocheng City.

1 Introduction

Land subsidence is an environmental geological phenomenon caused by natural or human factors, which consolidates and compresses the surface soil of the earth's crust and leads to a slow decrease in regional ground elevation[1]. It has the characteristics of slow generation, long duration, wide impact range, complex genetic mechanism, and high difficulty in prevention and control[2-4]. The main reasons for ground subsidence include the exploitation of underground fluids and the extraction of solid minerals[5,6], which causes the compressive deformation of the soil skeleton under the action of top loading. Ground subsidence center funnel area and groundwater level flow field maps in Liaocheng City basically coincide with each other. Therefore, it can be preliminarily concluded that the main cause of ground subsidence in Liaocheng City is the over-exploitation of groundwater.of land subsidence.

A. M. Zende et al. (eds.), *Proceedings of the 2024 3rd International Conference on Structural Seismic Resistance, Monitoring and Detection (SSRMD 2024)*, Atlantis Highlights in Engineering 27,
https://doi.org/10.2991/978-94-6463-404-4_33

In terms of geographical distribution, the land subsidence areas in China are mainly concentrated in the Yangtze River Delta, the Yellow-Huai-Hai Plain, the Song-Nan Plain, the Southeast Coastal Plain, the river valley plains and mountain basins[7-10]. At present, the North China Plain is the region with the largest area affected by land subsidence and the fastest subsidence rate in China. The land subsidence in Shandong Province is mainly distributed in the northwest plain of Shandong, specifically in areas such as Dezhou, Dongying, Binzhou, Liaocheng, and Jining. Among them, the areas with the most severe land subsidence in Liaocheng City are distributed in Linqing, Guanxian, Chiping, and Dong'a, with an average subsidence rate of 30-50mm/a. To prevent land subsidence in this area from causing significant impacts on urban planning and construction, socio-economic development, and people's lives, it is necessary to conduct systematic research and analysis on the phenomenon of land subsidence.

Based on the hydrogeological and engineering geological data and historical land subsidence monitoring data of Liaocheng City[11-14], we established a coupled flow-solid numerical model of land subsidence in Liaocheng. The model was used to restore the evolution law of land subsidence caused by excessive groundwater exploitation, and predict the future development trend of land subsidence, so as to propose targeted land subsidence prevention and control plans.

2 Study Area

Liaocheng is located in the western part of Shandong Province, at the junction of Hebei, Shandong, and Henan provinces, with a total area of 8628 km^2. Its geographical location is shown in Figure 1. To the west is the Zhangwei River, facing the Handan and Xingtai regions of Hebei Province across the water. To the south and southeast are the Jindi River, the Yellow River, and Henan Province, as well as the cities of Jining, Tai'an, and Jinan in this province. To the north and northeast are the borders of Dezhou City. The geographical coordinates are 35°47′N~37°03′N and 115°16′E~116°32′E. The straight-line distance from east to west is 114 km and from north to south is 138 km. The study area has a warm-temperate monsoon climate with four distinct seasons. The average annual precipitation is about 650 mm, concentrated from June to August.

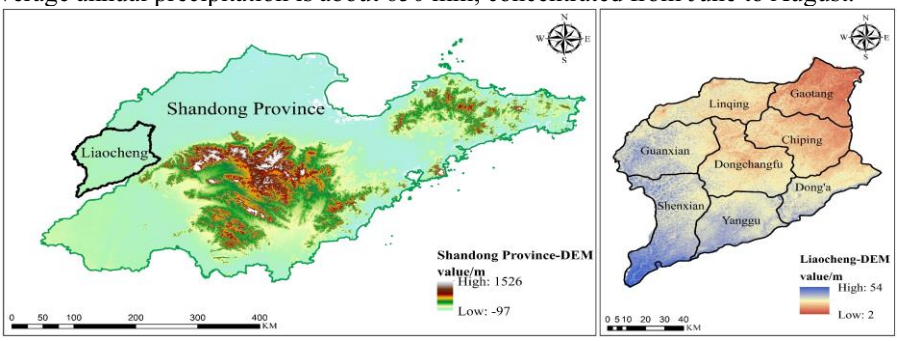

Fig. 1. Geographical location map of the study area

Based on the relevant investigation data in the study area, the groundwater system in the region is divided into three water-bearing rock layers from top to bottom, namely shallow, medium-deep and deep layers. The shallow freshwater rich zone is mainly distributed in the mainstream zone of ancient river channels, and the bottom interface is deeply buried. The aquifer has a large thickness, abundant water volume, and good water quality, mainly distributed in the urban areas of Dong'a, Dongchangfu, Guanxian, Shenxian, and Linqing. Due to the constraints of ancient geographical environment, the groundwater in the medium deep layers of water-bearing rock formations is mainly composed of saline water (except for some completely depleted areas). Currently, the groundwater in this layer has no utilization value. The lithology of the deep water-bearing rock formation is composed of silt, fine sand, medium fine sand, medium sand, medium coarse sand, coarse sand, and gravel mixed with coarse sand. However, it is mainly composed of medium fine sand, and there are relatively stable aquifers above and below the aquifer.

3 Method

Soil consolidation and water depletion is a typical example of fluid-solid interaction in porous materials, which is microscopically characterized by interactions between seepage and stress fields[15]. A three-dimensional interactive model of fluid and solid dynamics was developed using groundwater movement and soil compression theory. The model was designed to predict the progression of land subsidence in the study area due to groundwater extraction.

3.1 Biot consolidation theory

Assuming that the soil is homogeneous, saturated and continuous, that the soil particles and pore water are incompressible, that the pore water seepage conforms to Darcy's law, and that the permeability and compression coefficients of the soil are constant during infiltration, the mathematical equation can be expressed as:

$$\begin{cases} -G\nabla^2 w_x - \frac{G}{1-2v}\frac{\partial}{\partial x}\left(\frac{\partial w_x}{\partial x}+\frac{\partial w_y}{\partial y}+\frac{\partial w_z}{\partial z}\right)+\frac{\partial u}{\partial x}=0 \\ -G\nabla^2 w_y - \frac{G}{1-2v}\frac{\partial}{\partial y}\left(\frac{\partial w_x}{\partial x}+\frac{\partial w_y}{\partial y}+\frac{\partial w_z}{\partial z}\right)+\frac{\partial u}{\partial y}=0 \\ -G\nabla^2 w_z - \frac{G}{1-2v}\frac{\partial}{\partial z}\left(\frac{\partial w_x}{\partial x}+\frac{\partial w_y}{\partial y}+\frac{\partial w_z}{\partial z}\right)+\frac{\partial u}{\partial z}=-\gamma \end{cases} \tag{1}$$

$$\frac{\partial}{\partial t}\left(\frac{\partial w_x}{\partial x}+\frac{\partial w_y}{\partial y}+\frac{\partial w_z}{\partial z}\right)+\frac{1}{\gamma_w}\left[\frac{\partial}{\partial x}\left(k_x\frac{\partial u}{\partial x}\right)+\frac{\partial}{\partial y}\left(k_y\frac{\partial u}{\partial y}\right)+\frac{\partial}{\partial z}\left(k_z\left(k_y\frac{\partial u}{\partial z}+\gamma_w\right)\right)\right]=0 \tag{2}$$

Where G is the shear modulus; ∇^2 is the Laplace operator, $\nabla^2=\frac{\partial^2}{\partial x^2}+\frac{\partial^2}{\partial y^2}+\frac{\partial^2}{\partial z^2}$; k_x, k_y, k_z are the permeability coefficients in the x, y, and z directions, respectively; w_x, w_y, w_z are the displacement components in the x, y, and z directions, respectively;

γ, γ_w are the weight of soil and water, respectively; v is the Poisson's ratio; u is the pore water pressure.

3.2 Solution conditions

3.2.1 Initial conditions.

At the initial moment, the seepage field, displacement field, and pore water pressure of the soil layer are:

$$p(x, y, z, t)|_{t=0} = p_0(x, y, z) \tag{3}$$

$$W(x, y, z, t)|_{t=0} = W_0 \tag{4}$$

$$\varphi(x, y, z, t)|_{t=0} = \varphi_0 \tag{5}$$

Where p_0 is the original formation pore water pressure; W_0 is the initial displacement of the soil body, which can be taken as 0; φ_0 is the initial porosity of the soil layer.

3.2.2 Boundary conditions.

The commonly used seepage field boundaries are the constant pressure boundary and the constant flow boundary, which can be represented as:

$$p(x, y, z)|_{\Gamma} = p_b \tag{6}$$

$$\int -\frac{k}{\mu} \nabla p \cdot \boldsymbol{n} \mathrm{d}\Gamma = q \tag{7}$$

Where p_b is the boundary Γ pore water pressure on the boundary; n is the boundary Γ normal vector of the boundary; q is the boundary Γ the known flow rate.

3.3 Model building

Based on the geological conditions, groundwater data, drilling data, and mining well location related data of the study area, the stratigraphy in this study are divided into 4 aquifers and 3 confined aquifers, as shown in Figure 2(a). The parameters of the layers were determined based on the relevant engineering geological survey reports of the study area and combined with the values from the *Engineering Geological Manual* (*Fifth Edition*). As show as Table 1.

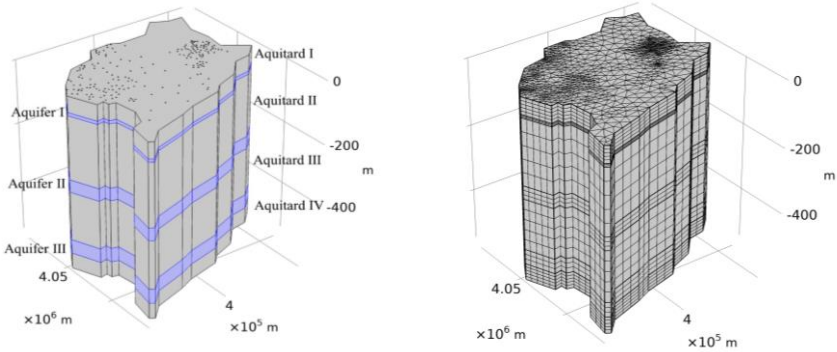

(a) (b)

Fig. 2. (a) Stratigraphic map of COMSOL model in Liaocheng and (b)model grid partitioning

Table 1. of Physical and Mechanical Parameters for Each Layer

Layer	depth of stratigraphy (m)	Elastic modulus (MPa)	Poisson ratio (1)	Density (kg/m^3)	Porosity (1)	Compression coefficient (MPa^{-1})
Aquitards I	0~-50	55	0.37~0.42	1977~1983	0.357~0.790	0.18~0.32
Confined aquifer I	-50~-60	75	0.22~0.27	1989~1997	0.359~0.758	-
Aquitards II	-60~-260	70	0.30~0.40	2032~2049	0.347~0.490	0.11~0.17
Confined aquifer II	-260~-300	80	0.21~0.27	2053~2059	0.367~0.721	-
Aquitards III	-300~-455	65	0.25~0.35	2065~2073	0.311~0.672	0.09~0.15
Confined aquifer III	-455~-500	65	0.27~0.32	2067~2077	0.327~0.701	-
Aquitards IV	-500~-550	65	0.25~0.32	2070~2080	0.355~0.365	0.025~0.027

The initial displacement of the model is set as 0, the bottom is set as fixed constraint, which limits the movement in the horizontal and vertical directions, the upper surface is set as free moving surface, and the surrounding area is set as roll support constraint, that is, there is displacement only in the vertical direction. The around boundary is set as the flow boundary and the head boundary, the hydraulic change conditions are obtained through the dynamic analysis of the groundwater flow field, and the extraction wells use flow boundary conditions to convert the actual amount of water extracted into mass fluxes.

The model boundary is made of multiple line segments as a representation of the reality boundary. The grid is divided into 113854 domain units, 36744 boundary units,

and 7446 edge units using a free triangular grid. The model grid is shown in Figure 2(b).

3.4 Verification of model accuracy and effectiveness

Using GIS spatial analysis technology, the InSAR monitoring results of land subsidence from 2017 to 2021 are superimposed and analyzed, and the 2017-2021 Liaocheng cumulative land subsidence development zoning map (Figure 3(a)) is obtained. According to three-dimensional numerical simulation experiments, the numerical simulation results of land subsidence in Liaocheng from 2017 to 2021 are shown in Figure 3(b).

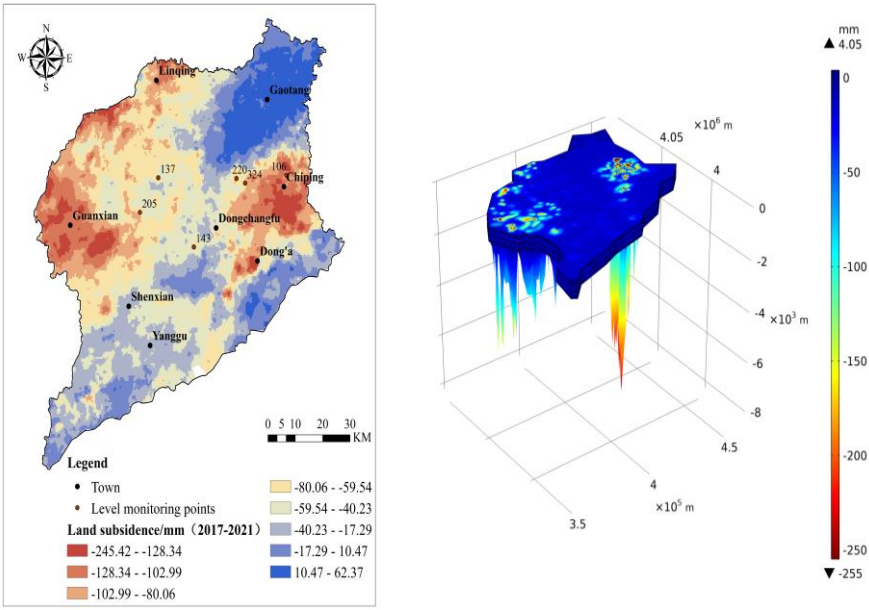

(a) (b)

Fig. 3. (a)Distribution Map of Land Subsidence in Liaocheng from 2017 to 2021 and (b) Numerical Simulation of Land Subsidence in Liaocheng from 2017 to 2021

Currently, there are 34 monitoring points within the scope of Liaocheng City, mainly distributed in Liaocheng District, Shen County, and Yanggu County. The monitoring data are the cumulative sedimentation amount from 2017 to 2021. Select some monitoring control points for statistical comparison and analysis of the actual settlement and the calculation results are shown in Table 2.

Table 2. Comparison of some settlement monitoring values and numerical simulation values in Liaocheng

Monitoring points		2017~2018		2018~2019		2019~2020		2020~2021	
		Settlement amount (mm)	Simulation error (%)	Settlement amount (mm)	Simulation error (%)	Settlement amount (mm)	Simulation error (%)	Settlement amount (mm)	Simulation error (%)
106	Measured value	-46	5.43	-22	10.45	-27	7.41	-23	4.78
	Simulated values	-43.5		-19.7		-29		-21.9	
137	Measured value	-38	7.89	-8	8.75	-8	8.75	13	12.31
	Simulated values	-35		-7.3		-7.3		14.6	
143	Measured value	-34	12.53	-7	8.57	-9	6.67	24	7.92
	Simulated values	-29.74		-7.6		-8.4		22.1	
205	Measured value	-45	3.67	-9	8.89	-14	4.29	5	8
	Simulated values	-43.35		-8.2		-13.4		4.6	
220	Measured value	-34	9.41	-27	5.19	-24	6.67	-2	6
	Simulated values	-37.2		-25.6		-22.4		-2.12	
324	Measured value	-39	12.31	-23	5.65	-23	12.17	-4	7.5
	Simulated values	-43.8		-21.7		-25.8		-3.7	

Comparing the monitoring values and simulation values, it can be concluded that the absolute simulation error has a minimum value of 3.67% and a maximum value of 12.53%. It shows that the numerical model can better describe the development trend of land subsidence in this area.

4 Prediction of Land Subsidence

4.1 Prediction of land subsidence under present exploration conditions

The land subsidence and groundwater extraction in 2021 were used as initial conditions to predict the development of ground subsidence in the study area in the next decade based on the numerical model developed. The results are shown in Figure 4.

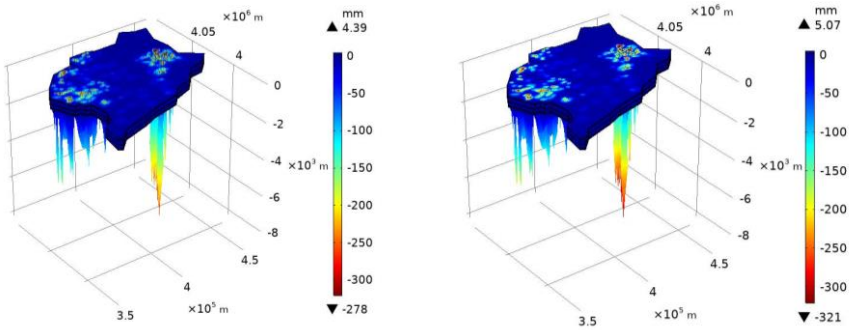

(a)2026 (b)2031

Fig. 4. Predicted land subsidence in 2026 and 2031

From the analysis of Fig. 4, it can be seen that if the current state of mining is maintained, the land subsidence in the study area will further develop, and the maximum subsidence will reach 321mm by 2031, which is 1.3 times of the maximum subsidence in 2021. At the same time, two large ground subsidence funnels will be formed in the east and west of Liaocheng City in 2031, and the subsidence range has a tendency to expand gradually to the surrounding area. After the formation of the ground subsidence funnels, land subsidence will further develop even without large-scale groundwater mining and other activities, a phenomenon known as "passive subsidence", to which special attention should be paid in the prevention and control of land subsidence.

4.2 Prediction of Land Subsidence under Prohibited Groundwater Extraction Conditions

In order to solve the contradiction between the people's growing needs for a better life and the rapid development of land subsidence disasters, according to the current mining output of each exploitation well in the study area, three areas with serious land subsidence in the study area were selected as the forbidden mining areas (A, B, C), and strictly comply with the requirements for the closure of each exploitation well in the area, as shown in Figure 5(a).

By simulating the fluid-solid coupling model of land subsidence in Liaocheng City, the distribution map of land subsidence in the study area in 2031 was obtained when the mining ban measures were taken (Figure 5(b)), and the impact of the mining ban on land subsidence in the study area was analyzed.

From the comparison of the figures, it shows that after effective mining bans are implemented in the main subsidence areas, the subsidence trend will undergo significant changes. The area where mining is prohibited has significantly slowed down its land subsidence. Moreover, under the conditions of mining prohibition, the maximum cumulative land subsidence in the study area in 2031 has also decreased compared to the current mining conditions, from 321mm to 256mm. The implementation of a ban on groundwater mining in a particular area will not only slow down the trend of ground subsidence in the area where mining is banned, but will also improve subsidence in the

surrounding areas. Therefore, it is effective to adopt a mining ban for areas with serious ground subsidence.

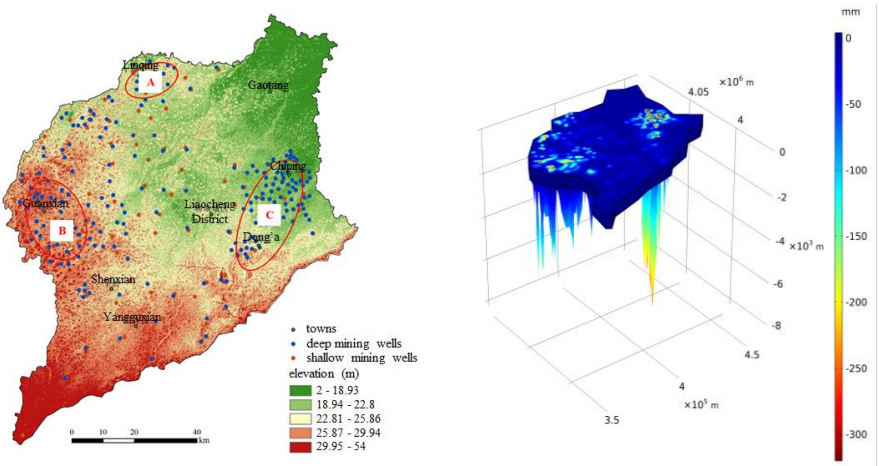

(a) (b)

Fig. 5. Schematic diagram of the division of prohibited mining areas in the research area and prediction of land subsidence in the study area in 2031

5 Conclusion

(1) According to the results of three-dimensional fluid-solid coupling numerical simulation, land subsidence in Liaocheng mainly occurs in four subsidence zones centered on Linqing, Guanxian, Chiping and Dong'a counties, with an average subsidence rate of about 30-50 mm/a. And the maximum cumulative land subsidence in Liaocheng will reach 321 mm in 2031.

(2) It is recommended to reduce the exploitation of groundwater and establish no-mining zones in Chiping, Linqing, Guanxian, and Dong'a counties, which will effectively curb the development of land subsidence. At the same time the subsidence trend in the areas near the subsidence funnel should be slowed down to prevent it from connecting into a larger subsidence area.

References

1. Zeng, C., et al., Combined recharge: A method to prevent ground settlement induced by redevelopment of recharge wells. *JOURNAL OF HYDROLOGY*, 2019. 568: p. 1-11.
2. Haghighi, M.H. and M. Motagh, Ground surface response to continuous compaction of aquifer system in Tehran, Iran: Results from a long-term multi-sensor InSAR analysis. *REMOTE SENSING OF ENVIRONMENT*, 2019. 221: p. 534-550.

3. Jia, X., et al., Groundwater depletion and contamination: Spatial distribution of groundwater resources sustainability in China. *SCIENCE OF THE TOTAL ENVIRONMENT*, 2019. 672: p. 551-562.
4. Rahmati, O., et al., Land subsidence hazard modeling: Machine learning to identify predictors and the role of human activities. *JOURNAL OF ENVIRONMENTAL MANAGEMENT*, 2019. 236: p. 466-480.
5. Herrera-Garcia, G., et al., Mapping the global threat of land subsidence. *SCIENCE*, 2021. 371(6524): p. 34-36.
6. Benveniste, J., et al., Requirements for a Coastal Hazards Observing System. *FRONTIERS IN MARINE SCIENCE*, 2019. 6.
7. Nicholls, R.J., et al., A global analysis of subsidence, relative sea-level change and coastal flood exposure. *NATURE CLIMATE CHANGE*, 2021. 11(4): p. 338-U82.
8. Wu, Y., et al., Analyses of leakage effect of waterproof curtain during excavation dewatering. *JOURNAL OF HYDROLOGY*, 2020. 583.
9. Wang, X., et al., Evaluation of optimized depth of waterproof curtain to mitigate negative impacts during dewatering. *JOURNAL OF HYDROLOGY*, 2019. 577.
10. Delgado Blasco, J.M., et al., Measuring Urban Subsidence in the Rome Metropolitan Area (Italy) with Sentinel-1 SNAP-StaMPS Persistent Scatterer Interferometry. *REMOTE SENSING*, 2019. 11(2).
11. Cigna, F. and D. Tapete, Present-day land subsidence rates, surface faulting hazard and risk in Mexico City with 2014-2020 Sentinel-1 IW InSAR. *REMOTE SENSING OF ENVIRONMENT*, 2021. 253.
12. Ghorbanzadeh, O., et al., A new GIS-based technique using an adaptive neuro-fuzzy inference system for land subsidence susceptibility mapping. *Journal of Spatial Science*, 2020. 65(3): p. 401-18.
13. Rahmati, O., et al., Land subsidence modelling using tree-based machine learning algorithms. *SCIENCE OF THE TOTAL ENVIRONMENT*, 2019. 672: p. 239-252.
14. Bierkens, M.F.P. and Y. Wada, Non-renewable groundwater use and groundwater depletion: a review. *ENVIRONMENTAL RESEARCH LETTERS*, 2019. 14(6).
15. Wang, Y., Z. Wang and W. Cheng, A review on land subsidence caused by groundwater withdrawal in Xi'an, China. *BULLETIN OF ENGINEERING GEOLOGY AND THE ENVIRONMENT*, 2019. 78(4): p. 2851-2863.